SCIENCE CHINA
Earth Sciences

•ARTICLE•

https://doi.org/10.1007/s11430-023-1326-2

Adaptive strategies of high and low nucleic acid prokaryotes in response to declining resource availability and selective grazing by protozoa

Chen HU[1,2,3], Liuqian YU[4], Xiaowei CHEN[2,3], Jihua LIU[5], Yao ZHANG[2,3], John BATT[3,6], Xilin XIAO[1,2,3], Qiang SHI[3,6], Rui ZHANG[2,7], Tingwei LUO[2,3,8], Nianzhi JIAO[2,3*] & Dapeng XU[2,3*]

[1] *College of the Environment and Ecology, Xiamen University, Xiamen 361102, China;*
[2] *State Key Laboratory of Marine Environmental Science, College of Ocean and Earth Sciences, Fujian Key Laboratory of Marine Carbon Sequestration, Xiamen University, Xiamen 361102, China;*
[3] *Joint Lab for Ocean Research and Education (LORE) of Dalhousie University, Canada, and Shandong University and Xiamen University, Xiamen 361102, China;*
[4] *Earth, Ocean and Atmospheric Sciences Thrust, The Hong Kong University of Science and Technology (Guangzhou), Guangzhou 510000, China;*
[5] *Institute of Marine Science and Technology, Shandong University, Qingdao 266237, China;*
[6] *Department of Oceanography, Dalhousie University, Halifax, Nova Scotia B3H 4R2, Canada;*
[7] *Institute for Advanced Study, Shenzhen University, Shenzhen 518060, China;*
[8] *Carbon Neutral Innovation Research Center, Xiamen University, Xiamen 361102, China*

Received September 21, 2023; revised April 9, 2024; accepted April 17, 2024; published online April 26, 2024

Abstract Prokaryotes play a fundamental role in global ocean biogeochemical cycles. However, how the abundance and metabolic activity of ecologically distinct subgroups (i.e., high nucleic acid (HNA) and low nucleic acid (LNA) cells), and their regulating factors, change in response to changing marine environmental conditions remains poorly understood. Here, we delved into the time-evolving dynamic responses of the HNA and LNA prokaryotic subgroups to declining resource availability and selective grazing by protozoa by conducting a 73-day incubation experiment in a large-volume (117,000 L) macrocosm that facilitates community-level exploration. We found that the metabolic activity of the HNA subgroup was higher than that of the LNA subgroup when the macrocosm was resource replete but that the HNA subgroup declined more rapidly than the LNA subgroup as the resources became increasingly scarce, leading to a steadily increasing contribution of LNA cells to prokaryotic activity. Meanwhile, as resources in the macrocosm became limited, protozoan grazing preference shifted from the HNA to the LNA subgroup and the contributions of the LNA subgroup to the carbon flow within the macrocosm increased. The findings highlight the resilience of LNA cells in resource-limited environments, illuminate the critical role of selective grazing by protozoa in balancing distinct prokaryotic subgroups under changing resource conditions, and demonstrate the complex and adaptive interactions between protozoa and prokaryotes across diverse environmental contexts.

Keywords Microbial loop, Macrocosm experiment, Prokaryote, Top-down and bottom-up controls, Carbon flow

Citation: Hu C, Yu L, Chen X, Liu J, Zhang Y, Batt J, Xiao X, Shi Q, Zhang R, Luo T, Jiao N, Xu D. 2024. Adaptive strategies of high and low nucleic acid prokaryotes in response to declining resource availability and selective grazing by protozoa. Science China Earth Sciences, 67, https://doi.org/10.1007/s11430-023-1326-2

* Corresponding authors: Dapeng XU (dapengxu@xmu.edu.cn), Nianzhi JIAO (jiao@xmu.edu.cn).

1. Introduction

Prokaryotes are the most substantial living biomass reservoir (Suttle, 2007) and integral constituents of the microbial loop in aquatic ecosystems (Azam et al., 1983). Prokaryotes also play a fundamental role in global ocean biogeochemical cycles. Given this essential role, even minor alterations in prokaryotic abundance and metabolic activity can profoundly impact the structure and function of marine ecosystems (Edwards and Richardson, 2004; Morán et al., 2010). Therefore, understanding how prokaryotic abundance and metabolic activity, and their regulating factors, respond to changes in the marine environment is critical to accurately predict future ocean ecosystem changes.

Prokaryotic abundance and metabolic activity are controlled by both bottom-up factors such as resource availability (Kirchman, 2008) and top-down factors such as mortality caused by grazing or lysis (Sanders et al., 1992; Thingstad and Lignell, 1997). Among the top-down factors, protozoa (notably flagellates and ciliates) are the most important grazers (Sieburth et al., 1978; Worden et al., 2015). They significantly influence prokaryotic abundance, community composition, and metabolic activity, and the transfer of energy and nutrients along the microbial loop to the upper trophic levels; they also act as an essential link in the marine food web (Azam et al., 1983). In estuaries (Painchaud et al., 1996) and offshore areas (Unrein et al., 2007; Pearce et al., 2010), protozoan grazing can contribute to as much as 100% of the prokaryotic mortality.

Selective grazing, where protozoa selectively graze on moderate-sized taxa over oversized or undersized taxa, has been proposed as a mechanism by which protozoa contribute to prokaryotic community succession (Pernthaler, 2005). In addition to the size-based grazing preference, selective grazing can be triggered by the metabolic activity of the prey (Sintes and Giorgio, 2014). For example, two subgroups of prokaryotes with different nucleic acid contents as determined by flow cytometry, namely high nucleic acid (HNA) cells and low nucleic acid (LNA) cells, display markedly distinct physiological, ecological, and metabolic characteristics (Li, 1995; Gasol and Morán, 1999; Bouvier and Giorgio, 2007; Hu et al., 2020). Previous studies have revealed that protozoa tend to graze on the metabolically more active HNA cells (Gonzalez et al., 1990; del Giorgio et al., 1996; Sintes and del Giorgio, 2014; Hu et al., 2020). In contrast, the diminutive size and reduced metabolic rates of LNA cells, enable them to persist and prevail under pronounced grazing pressure (Segovia et al., 2018). However, the degree of selective grazing by protozoa may be affected by many factors, such as the abundance of bioavailable resources. For instance, Baltar et al. (2016) observed that the protozoan grazing pressure in a simulated algal bloom culture environment intensified with increasing nutrient levels and significantly impacted bacterial abundance. Hu et al. (2020) showed that protozoa displayed a marked preference for the HNA subgroup over the LNA subgroup in the nutrient-rich coastal regions off the Pearl River Estuary, whereas such selective grazing waned as the ambient nutrient concentrations decreased with increasing distance from the estuary to the open ocean.

Collectively, previous studies have demonstrated the intricate interactions between selective grazing by protozoa and the metabolic activity of prokaryotes under different levels of resource availability. However, some investigations were conducted in a small-volume incubation system, which is prone to the "bottle effect", where the limited size of the closed incubation system significantly influences microbial growth and fails to accurately mimic the dynamics of the natural environment. In addition, some studies were field surveys, which capture only a snapshot in time and rely on correlational inferences to deduce causal relationships among nutrient resources, prokaryotes, and protozoa.

To overcome these limitations, we conducted a 73-day incubation experiment in a large-volume (117,000 L) macrocosm, which avoids the bottle effect and allows time-series sampling and analysis of various parameters. Throughout the incubation, we analyzed the time-evolving dynamics of resource availability, prokaryotic abundance and activity, protozoan grazing-mediated mortality of the HNA and LNA subgroups, potential carbon production during prokaryotic growth, and carbon lost mediated by protozoan grazing. This comprehensive analysis allowed us to confirm whether protozoa exert selective grazing pressure on distinct prokaryotic taxa, specifically the HNA and LNA subgroups, and how the efficacy of selective grazing fluctuates with changes in bioavailable nutrient levels. Subsequently, we constructed a diagram of carbon flow within the incubation system to quantify the contributions of distinct prokaryotic groups to carbon flow within the microbial loop. The findings illuminate the role of selective grazing by protozoa in balancing the HNA and LNA subgroups under changing resource conditions, which is crucial for the stability and efficiency of the microbial loop, and highlight the complex and adaptive interactions between protozoa and prokaryotes across diverse environmental contexts.

2. Materials and methods

2.1 Experimental setup and measurement of environmental parameters

The Aquatron Tower Tank, a large-volume indoor macrocosm situated at Dalhousie University in Canada, was used as the incubation system. The tank is 10.6 meters in height and 3.7 meters in diameter, holding approximately 117,000 L

of natural seawater (Appexdix Figure S1, https://link.springer.com). The seawater was collected from the Halifax coastal sea (44°37′1.77″N, 63°33′23.86″W), promptly filtered through a 300-μm mesh, and then filled into the tank. The enclosed macrocosm was incubated in darkness, under ambient temperature, and without external input for a total of 73 days, from September to December 2017. Throughout the incubation period, samples for further analyses were collected from the surface (1 m) and bottom (9 m) layers of the tank, with a high sampling frequency of approximately every 2 to 4 days during the first 16 days and nearly every week thereafter. The biological samples, namely those for measuring prokaryote and nanoflagellate abundance and dilution experiments, were pre-filtered through a 20-μm mesh to remove larger particles and plankton.

Vertical profiles of temperature, salinity, and dissolved oxygen (DO) concentrations in the entire water column of the tank were recorded every 2 days throughout the incubation period using a Multiparameter Sonde (YSI EXO, YSI Incorporated, USA). Concentrations of inorganic nutrients at the surface and bottom layers, including ammonium (NH_4^+), nitrite (NO_2^-), nitrate (NO_3^-), silicate (SiO_4^{4-}), and phosphate (PO_4^{3-}), were measured in triplicate samples using a Skalar SAN++ autoanalyzer, following previous methodologies (Shi and Wallace, 2018).

2.2 Microbial abundance

For the enumeration of prokaryotes, 2-mL subsamples were fixed with glutaraldehyde (0.5% final concentration) at room temperature for 15 min, followed by storage at –80°C after flash-freezing in liquid nitrogen. Autotrophic picoplankton, including Synechococcus and pigmented picoeukaryotes, were enumerated directly using flow cytometry (BD Accuri C6, USA) without staining, following an established protocol (Marie et al., 1999). The abundance of prokaryotes, including bacteria and archaea, was ascertained by staining with SYBR Green I (Molecular Probe, United States) and measuring the fluorescence by flow cytometry as described for picoplankton. Fluorescent beads (Molecular Probes) with a diameter of 1 μm were used as an internal standard during flow cytometric determination.

The HNA and LNA prokaryotic subgroups were distinguished based on their respective signatures in the cytogram plot of side scatter (SSC) versus green fluorescence, as delineated by Gasol et al. (1999). Flow cytometric data analysis was conducted using FlowJo vX.0.7 software (Tree Star, USA).

2.3 Nanoflagellate abundance and biomass

To quantify the abundance of heterotrophic nanoflagellates (HNF), the following steps were employed: 50-mL subsamples were fixed with glutaraldehyde to a final concentration of 1%, collected on 0.45-μm polycarbonate black filters, and stained with DAPI (4,6-diamidino 2-phenylindole) at a final concentration of 10 μg mL^{-1}, following established protocols (Sherr et al., 1993; Yang et al., 2020). HNF were counted along several transects using epifluorescence microscopy (Olympus BX51, Olympus America Inc., Center Valley, PA, USA) at ×1000 magnification. At least 50–100 HNF cells were counted in at least 25 fields per filter to ensure statistical rigor. HNF biovolumes were calculated from cell geometries as described by Pasulka et al. (2015), and carbon biomass was calculated according to Menden Deuer and Lessard (2000).

2.4 Dilution experiment and estimation of growth and mortality rates

A serial dilution technique was utilized to estimate prokaryotic gross growth and mortality mediated by protozoan grazing (Landry and Hassett, 1982; Jochem et al., 2004). Seawater was passed through a 20-μm mesh and subsequently filtered using a tangential flow filtration system with 0.2-μm pore size polyvinylidene difluoride cartridges (Labscale, Millipore, USA) to generate grazer-free diluents (Figure S2). The polycarbonate bottles used in the experiments were acid-cleaned with 10% HCl and rinsed thoroughly with Milli-Q water. The diluents were added to 250-mL polycarbonate bottles in proper proportions to create a t_0 dilution series consisting of 20%, 40%, 60%, and 100% whole seawater. For each t_0 bottle, triplicate 50-mL polycarbonate bottles were rinsed twice with the diluent and gently filled with the diluent via siphoning to minimize harm to grazers and prokaryotes. Following these preparatory steps, the 50-mL polycarbonate bottles (12 bottles in total for each experiment) were incubated at room temperature in the dark for 24 h. Triplicate 2-mL samples were collected at the beginning and end of the incubation to estimate prokaryotic abundance.

The net growth rate of the prokaryotes (k, d^{-1}) was calculated for each sample based on the prokaryotic abundance at the start (t_0) and the end (t) of the incubation experiment (N_0 and N_t, respectively), assuming exponential growth (Landry and Hassett, 1982; Jochem et al., 2004):

$$k = \frac{\ln \frac{N_t}{N_0}}{t - t_0}. \quad (1)$$

The slope of the regression of the net growth rate versus the dilution factor was interpreted as the protozoan grazing-mediated specific prokaryotic mortality rate (PMM). The prokaryotic gross specific growth rate (PGG) was determined as the y-intercept value of the regression line. PGG and PMM rates were calculated separately for the HNA and LNA prokaryotic subgroups.

2.5 Carbon production and losses

To calculate the daily quantities of carbon generated by prokaryotic production and carbon loss mediated by protozoan grazing, we assumed that the prokaryote population dynamics can be depicted by the following differential equation model (Landry et al., 1995; Biggs et al., 2021):

$$\frac{\mathrm{d}N}{\mathrm{d}t} = (\mathrm{PGG} - \mathrm{PMM})N, \tag{2}$$

where N represents prokaryotic abundance at time t.

Assuming that the specific growth and mortality rates remain constant over the adequately short time interval, the differential equation can be solved as follows:

$$N(t) = N_0 \mathrm{e}^{(\mathrm{PGG}-\mathrm{PMM})t}. \tag{3}$$

The total number of prokaryotic cells generated over a time span t (PA_t), assuming that PGG and PMM are unchanged within the time span, can be estimated by integrating the production rate over time:

$$\mathrm{PA}_t \equiv \int_0^{\mathrm{t}} \mathrm{PGG} \times \mathrm{N}(t)\mathrm{d}t. \tag{4}$$

Incorporating eq. (3) into eq. (4) and performing subsequent integration yields:

$$\mathrm{PA}_t = \frac{\mathrm{PGG}}{\mathrm{PGG}-\mathrm{PMM}}\left(N_0 \mathrm{e}^{(\mathrm{PGG}-\mathrm{PMM})t} - N_0\right). \tag{5}$$

Similarly, the total number of prokaryotic cells lost due to grazing over a time span t (PL_t) can be calculated as follows:

$$\mathrm{PL}_t = \frac{\mathrm{PMM}}{\mathrm{PGG}-\mathrm{PMM}}\left(N_0 \mathrm{e}^{(\mathrm{PGG}-\mathrm{PMM})t} - N_0\right). \tag{6}$$

We calculated daily rates of PA and PL, by selecting a time interval t=1 day, in line with the 24-h incubation period used in the dilution assays.

Furthermore, to convert cell numbers to prokaryotic biomass and obtain the prokaryotic gross bacterial production (PBP) and protozoan grazing-mediated carbon loss (PMC), the total number of cells produced and lost (i.e., PA and PL) were multiplied by the average carbon content of the prokaryotic cell (12.4 fg C cell^{-1}) determined from a previous investigation (Fukuda et al., 1998).

In this study, alterations in carbon flow due to other pathways were collectively accounted for by calculating the difference between PBP, PMC, and ΔBB, where ΔBB denotes the change in prokaryotic biomass during the incubation experiment.

2.6 Statistical analysis

Shapiro-Wilk W tests were utilized to assess data normality before analysis, and logarithm transformation was performed as necessary. A least-square regression analysis was conducted to examine the relationship between the net growth rate and fractions of the grazer-free dilution series. Significant differences between samples were determined using paired t-tests. The relationships between prokaryotic parameters (i.e., HNA and LNA abundance, PGG of the HNA and LNA subgroups (PGG-H and PGG-L, respectively), the ratio of LNA abundance to total prokaryotic abundance (LNA%), and the ratio of LNA gross growth rate to HNA gross growth rate (PGG-L/PGG-H)) and abiotic and biotic variables were scrutinized using Pearson's correlation analysis with a significance level (α) of 0.05. A linear regression model was employed to characterize the following: (1) the relationship among the abundances of HNA, LNA, and HNF, LNA%, and the incubation time during two different phases of the experiment (i.e., P1 and P2); (2) the relationship among PGG-H, PGG-L, PMM-H, PMM-L, PGG-L/PGG-H, and PMM-L/PMM-H and the incubation time during two different phases of the experiment (i.e., P1 and P2). GraphPad Prism 7 (GraphPad, USA) software was employed for the above statistical analyses. Redundancy analysis (RDA) was used to evaluate the variation in prokaryotic abundance and gross growth due to protozoan dynamics and environmental factors using R statistical software (R Development Core Team, 2012). The response variables were HNA and LNA abundance, PGG-H, PGG-L, and PGG-L/PGG-H, and the explanatory variables were HNF abundance, PMM-H, PMM-L, PMM-L/PMM-H, nitrogen nutrient concentrations (i.e., nitrite, nitrate, and ammonium), and DO. The significance of the axes was ascertained by Monte Carlo permutation tests with 9999 permutations. All tests were considered significant at P<0.05.

3. Results

3.1 Physical and chemical characteristics of the macrocosm

Throughout the incubation experiment, a stable hydrologic condition was maintained in the macrocosm, as evidenced by a nearly uniform vertical distribution of salinity (Figure S3a) and dissolved oxygen concentration (Figure S3c). In addition, other parameters such as temperature and nutrient concentrations showed similar changes over time in the surface and bottom layers. Specifically, surface and bottom temperature increased from 17.7 °C to a peak value of 20.5 °C on day 36 and then slightly dropped to 19.5 °C on day 48; the temperature then dropped to 18.3 °C and remained the same till the end of the incubation experiment (Figure S3b).. Surface and bottom nitrite concentrations remained low (<0.8 μmol L^{-1}) (Figure S4a). Ammonium concentrations decreased from 3.31–3.36 μmol L^{-1} to 0 μmol L^{-1} during the initial 40 days, and subsequently increased to 0.2 μmol L^{-1} in the surface layer and 0.36 μmol L^{-1} in the bottom layer (Figure S4b). Nitrate concentrations peaked on day 40 (10.40 μmol L^{-1}) and day

56 (10.56 μmol L^{-1}) in the surface and bottom layers, respectively (Figure S4c). Silicate and phosphate concentrations in the macrocosm ecosystem changed little throughout the incubation period (Figure S4d and S4e). More details about the temporal variations in temperature, salinity, and dissolved oxygen are described in Xiao et al. (2022), and variations in nutrients are described in Zhang et al. (2021).

3.2 Microbial abundance

HNA abundance varied significantly during the incubation period (Figure 1a), decreasing from initial values of (4.37–4.51)×10^5 cells mL^{-1} to (2.99±0.16)×10^5 cells mL^{-1} in the surface layer and (2.42±0.19)×10^5 cells mL^{-1} at the bottom layer on day 16. The cell number approximately doubled by day 20, and then progressively declined until day 73. Linear regression analysis at different incubation time periods revealed significant decreases for both days 0–16 (P<0.0001) and days 16–73 (P<0.0001) (Figure 1a).

Changes in LNA abundance largely mirrored those in HNA abundance, albeit with less fluctuations. The initial LNA abundance was (4.63±0.11)×10^5 cells mL^{-1} in the surface layer and (4.54±0.22)×10^5 cells mL^{-1} in the bottom layer, almost equivalent to the initial HNA abundance. The decrease in LNA abundance from day 0 to day 16 was smaller than that of HNA; there were (3.67–3.77)×10^5 cells mL^{-1} on day 16, which was higher than the number of HNA cells (Figure 1b). After day 16, LNA abundance slightly increased, followed by a dramatic drop on day 40 and a gradual decline for the remaining incubation period.

Conversely, HNF abundance in the surface and bottom layers gradually increased (P<0.003) from initial values of 295–336 cells mL^{-1} to a peak of 538–599 cells mL^{-1} on day 16, and then markedly decreased (P<0.001) to nearly half of the initial abundance (160–182 cells mL^{-1}) by the experiment's end (Figure 1c).

Intriguingly, the ratio of LNA abundance to total prokaryotic abundance (LNA%) significantly increased during the initial 0–16 days, from about 50% on day 1 to 55%–58% on day 16 (Figure 1d). LNA% dipped below 50% on day 20, but increased again, though moderately, throughout the remaining incubation period, approaching nearly 60% by the experiment's end.

Given the distinct variations in microbial abundance between incubation days 0–16 and 16–73, we present our analysis in two separate phases hereafter. Phase 1 (P1) encompasses the incubation period from day 0 to day 16 when nutrients were being depleted, while Phase 2 (P2) spans day 16 to day 73 when even more nutrients were being depleted.

3.3 Microbial activities

During P1 (days 0–16), the prokaryotic gross growth rate for the HNA subgroup (PGG-H) remained stable, fluctuating between 1.57–3.20 d^{-1}, peaking on day 4. The non-significant linear regression results indicated that the HNA subgroup was not resource-limited at this phase. However, during P2 (days 16–73), the PGG-H significantly decreased, as evidenced by the significant negative linear relationship between PGG-H and time (P=0.001) (Figure 2a). Conversely, the LNA subgroup's gross growth rate (PGG-L) oscillated during P1 and stabilized during P2. The PGG-L gradually decreased throughout the incubation process (P=0.02) but at a lower rate than PGG-H (Figure 2b).

The PGG-L/PGG-H ratio indicates the relative importance of the LNA and HNA subgroups to the activity of the prokaryotic community. PGG-L/PGG-H ranged from 0.07–0.22 during P1, suggesting that the HNA subgroup was the primary contributor to the prokaryotic activity. However, PGG-L/PGG-H increased to 0.6 during P2, revealing an increasingly larger contribution of the LNA subgroup to the total prokaryotic activity (Figure 2c).

The protozoan grazing-mediated mortality of the HNA subgroup (PMM-H) mirrored the changes in PGG-H, indicating a stable protozoan grazing pressure on the HNA subgroup during P1 (Figure 2d). In contrast, the grazing pressure of protozoa on the LNA subgroup (PMM-L) remained stable and fluctuated throughout the entire incubation, ranging from 0.10 to 0.25 d^{-1} (Figure 2e).

The PMM-L/PMM-H ratio reflects the strength of the selective grazing by protozoa on the LNA and HNA subgroups. During P1, the PMM-L/PMM-H was as low as 0.07 (surface layer on day 16), indicating that protozoa had a strong preference for the HNA subgroup. However, as the incubation experiment progressed, the PMM-L increased significantly (P=0.02), reaching 0.73 (bottom layer on day 64) (Figure 2f).

3.4 Abiotic and biotic drivers of prokaryotic abundance and activities

Pearson correlation analysis identified potential drivers of prokaryotic abundance and activities (Figure 3). During P1, HNA abundance was strongly and positively correlated with silicate concentration (r=0.5, P<0.05), nitrite concentration (r=0.80, P<0.05), DO concentration (r=0.57, P<0.05), ammonium concentration (r=0.6, P<0.05), and phosphate concentration (r=0.5, P<0.05), but negatively correlated with HNF abundance (r=–0.62, P<0.05). The abundance of the LNA subgroup exhibited similar relationships with all abiotic and biotic factors except for silicate concentration. LNA% showed analogous but inverse correlation results compared with those of HNA and LNA abundance, and it was positively correlated with HNF abundance (r=0.52, P=0.1). No significant relationship was found between prokaryotic activities (PGG) and environmental factors.

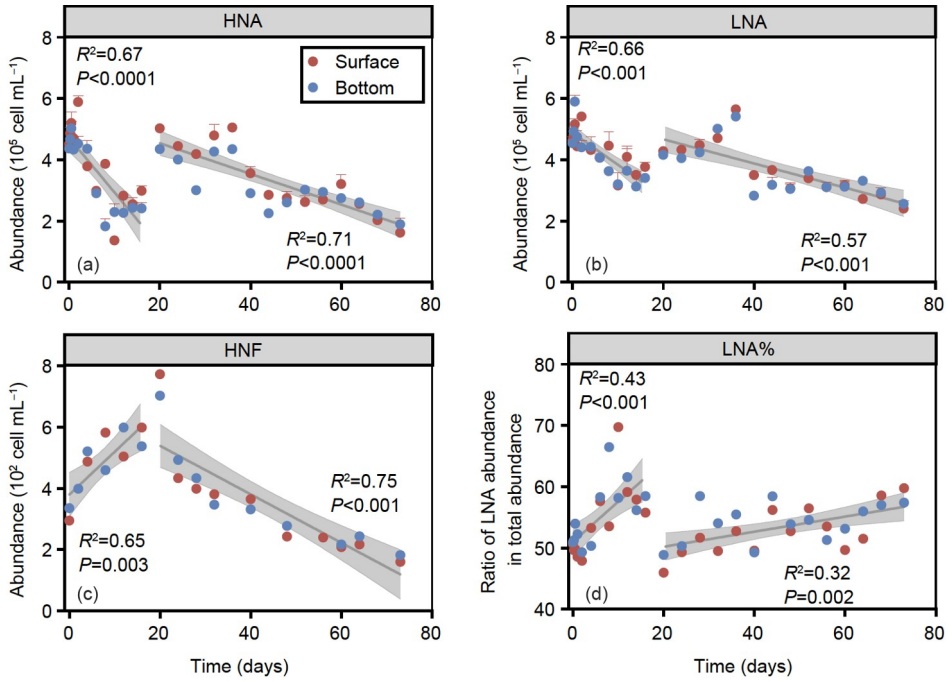

Figure 1 Dynamics of microbial abundance and the ratio of low nucleic acid (LNA) prokaryotic abundance to total prokaryotic abundance in the surface (red) and bottom (blue) layers of the Aquatron macrocosm. (a) High nucleic acid (HNA) prokaryote; (b) LNA prokaryote; (c) heterotrophic nanoflagellate (HNF) abundance; (d) the ratio of LNA abundance to total prokaryotic abundance (LNA%). The standard deviation is indicated by error bars. Regression analysis was performed separately for each data set during P1 (days 0–16) and P2 (days 16–73), and the regression results (R^2 and P) are shown next to the regression curves, with gray areas representing confidence intervals.

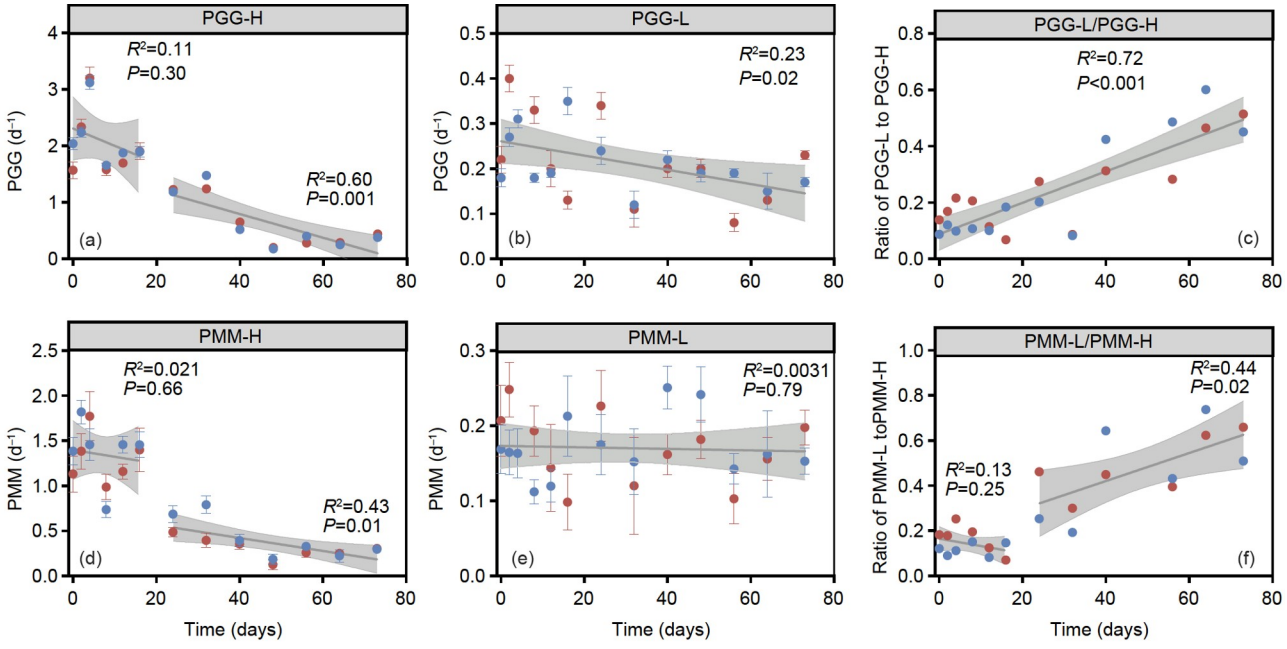

Figure 2 Dynamics of microbial activities and the ratio of LNA activities to HNA activities in the surface (red) and bottom (blue) layers of the Aquatron macrocosm. (a) Prokaryotic gross growth rate for HNA (PGG-H). (b) Prokaryotic gross growth rate for LNA (PGG-L). (c) The ratio of PGG-L to PGG-H (PGG-L/PGG-H). (d) Protozoan grazing-mediated HNA mortality rate (PMM-H). (e) Protozoan grazing-mediated LNA mortality rate (PMM-L). (f) The ratio of PMM-L to PMM-H (PMM-L/PMM-H). The standard deviation is represented by error bars. Regression analysis was performed separately for each data set during P1 (days 0–16) and P2 (days 16–73), and the regression results (R^2 and P) are shown next to the regression curves, with gray areas representing confidence intervals.

During P2, HNA and LNA abundance remained significantly and positively correlated with nitrite and ammonium concentrations but negatively correlated with nitrate concentration. HNF abundance correlated positively with

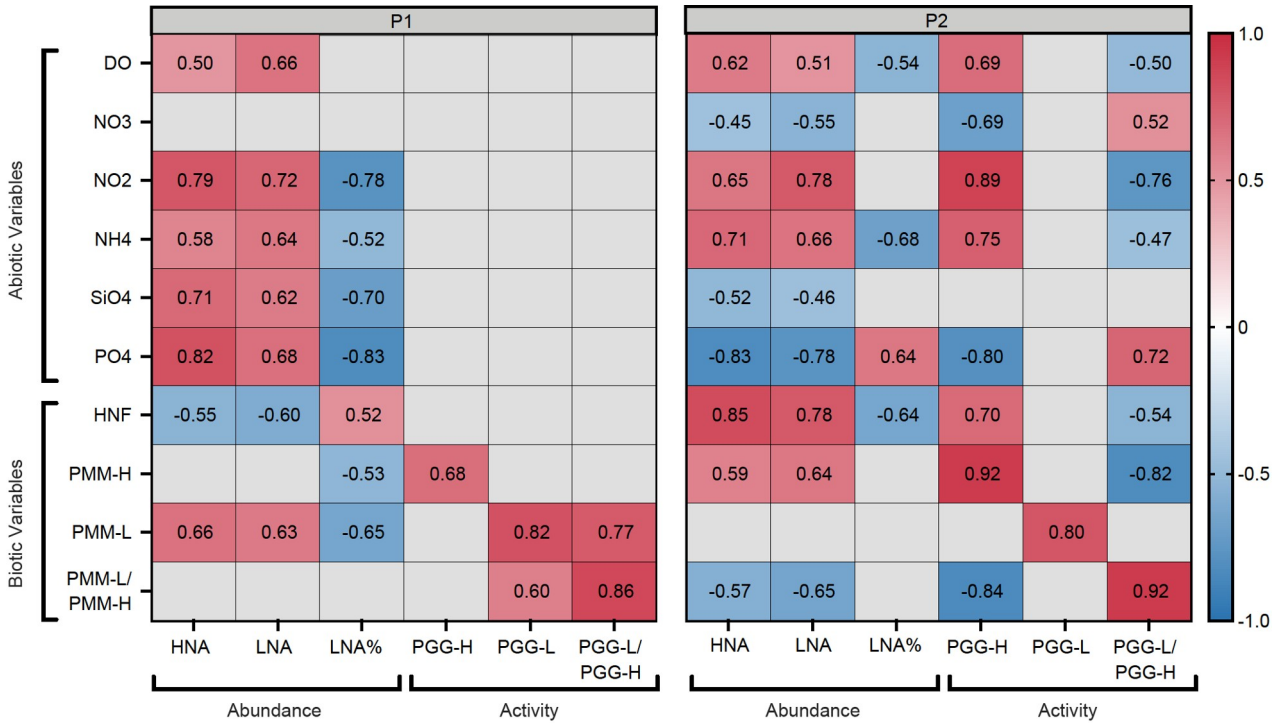

Figure 3 Pearson correlation coefficients between prokaryotic parameters (i.e., HNA and LNA abundances, the ratio of LNA abundance to total prokaryotic abundance (LNA%), gross growth rates of the HNA (PGG-H) and LNA (PGG-L) subgroups, and the ratio of PGG-L to PGG-H (PGG-L/PGG-H)) and abiotic (i.e., dissolved oxygen (DO), nitrite (NO_3), nitrate (NO_2), ammonium (NH_4), silicate (SiO_4), and phosphate (PO_4)) and biotic variables (i.e., HNF abundance, the protozoan grazing-mediated mortality of the HNA (PMM-H) and LNA (PMM-L) subgroups, and the ratio of PMM-L to PMM-H (PMM-L/PMM-H)) for Phase 1 (P1; days 0–16) and Phase 2 (P2; days 16–73).Only statistically significant correlations are shown (P<0.05).

both HNA and LNA abundance. LNA% was negatively correlated with DO and HNF abundance and positively correlated with phosphate. PGG-H correlated positively with bioavailable nitrite and ammonium concentrations, but there was no significant relationship between PGG-L and other abiotic factors. PMM-L/PMM-H exhibited negative correlations with prokaryotic abundance and PGG-H, whereas PGG-L/PGG-H was significantly and negatively correlated with nitrite and ammonium and positively correlated with nitrate, differing from the correlations observed during P1.

RDA was employed to further examine the potential effects of biotic and abiotic factors on changes in HNA and LNA subgroup abundance, gross growth rate, and relative contribution to the prokaryotic community throughout the incubation (Figure 4). The analysis revealed that variations in PMM-H, changes in protozoan grazing selectivity (characterized by PMM-L/PMM-H), and the interconversion between nitrate and nitrite were the primary factors affecting prokaryotic abundance, metabolic activity, and the relative contributions of the HNA and LNA subgroups throughout the incubation. Interestingly, distinct factors drove these changes during P1 and P2. During P1, PMM-H and PMM-L/PMM-H were the main factors responsible for changes in prokaryotic abundance and HNA metabolic activity. In contrast, during P2, the interconversion between nitrate and nitrite played a more significant role, influencing the changes in the relative contribution of the LNA subgroup to prokaryotic metabolic activity.

3.5 Alteration of carbon flow in the HNA and LNA subgroups

The prokaryotic gross bacterial production (PBP) and protozoan grazing-mediated carbon loss (PMC) of the HNA and LNA subgroups were estimated and compared to assess the channeling of carbon flow by prokaryotic activities during incubation, i.e., to determine whether the carbon cycling within the macrocosm was dominated by the HNA or LNA subgroup and what energy sources are needed for protozoa to maintain their survival (Figure 5).

The PBP of the HNA subgroup (PBP-H) exhibited a dynamic pattern during P1, peaking on day 4 (40.47–52.55 μg L^{-1} d^{-1}) and rapidly decreasing thereafter (7.54–12.53 μg L^{-1} d^{-1} on day 16). During P2, PBP-H slightly increased before declining rapidly, remaining at 1.01–1.82 μg L^{-1} d^{-1} during the end of P2 (Figure 5a). PMC of the HNA subgroup (PMC-H) mirrored PBP-H throughout the incubation (Figure 5b). Overall, an average of 67% of PBP-H was diverted through protozoan grazing on the HNA subgroup and transferred to upper trophic levels along the microbial loop.

In contrast, the PBP of the LNA subgroup (PBP-L) did not change as dramatically as PBP-H during the incubation,

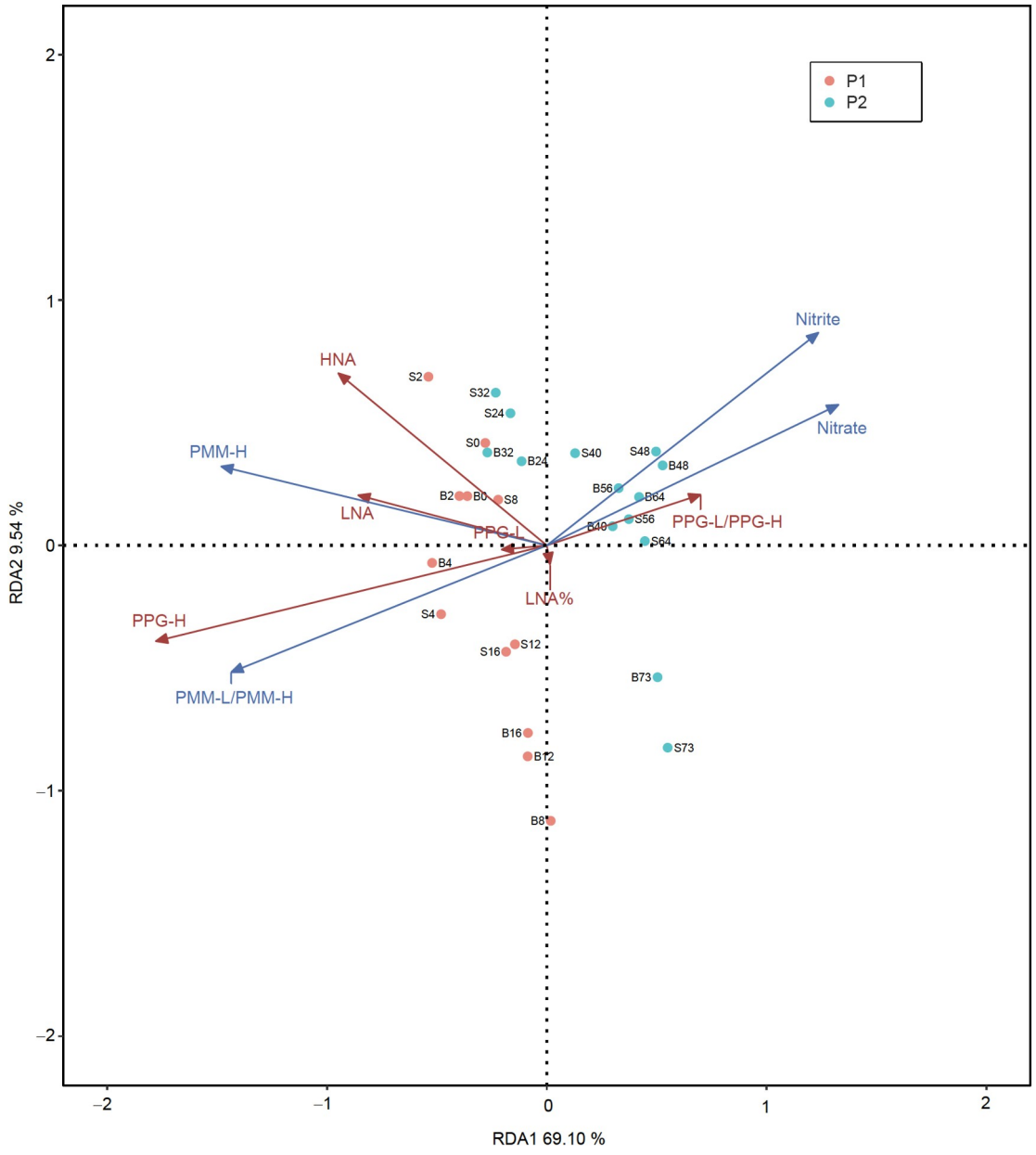

Figure 4 Redundancy analysis (RDA) reveals fluctuations in prokaryotic abundance and activities (response variables, in red) due to protozoan dynamics and environmental factors (explanatory variables, in blue). The numbers represent the sampling day and capital letters represent the sampling layer (i.e., S denotes the surface layer and B denotes the bottom layer) during the incubation period. Red and green dots mark the sampling days during Phase 1 (P1; days 0–16) and Phase 2 (P2; days 16–73), respectively. All explanatory variables in the RDA model were significant (P<0.05). The RDA model explains a total variation of 78.64%.

ranging from 0.76 to 5.1 μg L^{-1} d^{-1} (Figure 5c). However, during P2, the ratio of PBP-L to PBP-H progressively increased. Although the PMC of the LNA subgroup (PMC-L) remained relatively stable throughout the incubation, the ratio of PBP-L consumed by protozoa varied significantly. Approximately 69% of the PBP-L was consumed by protozoa during P1, similar to the fraction of PBP-H consumed by protozoa (Figure 5d). However, during P2, over 100% of PBP-L was allocated to protozoa, which is considerably higher than the percentage of PBP-H.

We further scrutinized the fluctuations in carbon flow through the microbial loop within the enclosed system during P1 and P2 (Figure 6). At the initial stage of the incubation, HNA and LNA biomasses were 8.51 μg L^{-1} and 6.99 μg L^{-1}, respectively. The average PBP reached 20.95 μg L^{-1} d^{-1}, with HNA metabolism contributing 91% and LNA a mere 9%. Moreover, the metabolic demand of protozoa was predominantly met from the consumption of HNA (11.25 μg L^{-1} d^{-1}) and, to a lesser degree, LNA (1.25 μg L^{-1} d^{-1}). The carbon budget balance (8.73 μg L^{-1} d^{-1}) was presumably released back into the environment, facilitating resource recycling. The energy transfer ratio, owing to

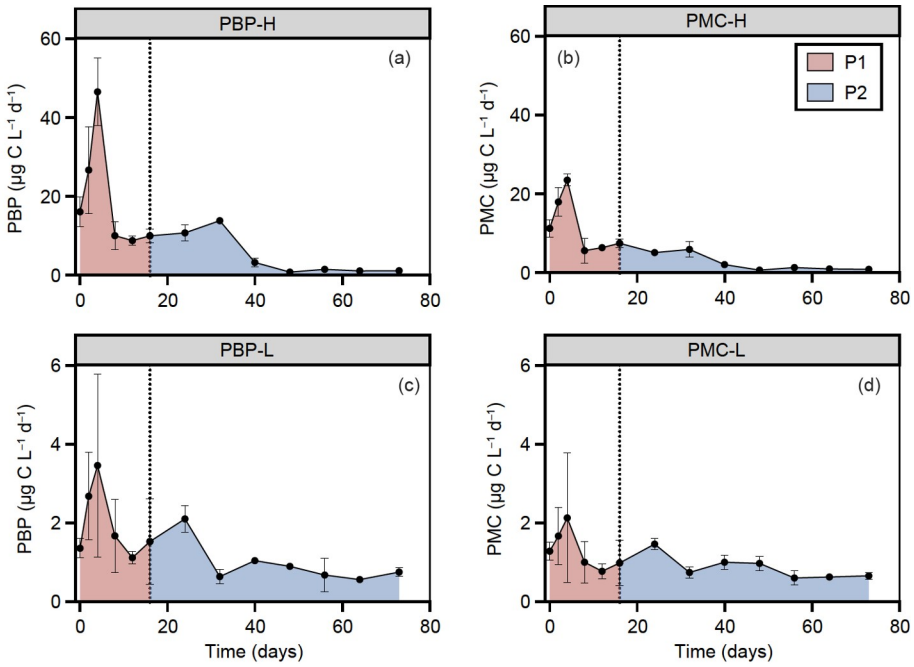

Figure 5 Carbon flow changes for the HNA and LNA subgroups during P1 (days 0–16) and P2 (days 16–73). PBP-H represents the prokaryotic gross bacterial production of the HNA subgroup (a), and PBP-L stands for the LNA subgroup (c). PMC-H indicates protozoan grazing-mediated carbon loss from the HNA subgroup (b), and PMC-L represents the LNA subgroup (d). The error bars indicate the standard deviation between the surface and bottom layer data.

protozoan grazing and resource recycling, reached 1.43 during P1.

Entering P2, the biomasses of HNA and LNA decreased to 2.60 μg L^{-1} and 3.66 μg L^{-1}, respectively. The average PBP-H decreased to 6.01 μg L^{-1} d^{-1}, representing a mere 32% of its value during P1. Conversely, the average PBP-L was 1.16 μg L^{-1} d^{-1}, which was 59% of its value during P1. Compared with P1, the contribution of LNA to prokaryotic gross production increased from 9% during P1 to 16% during P2, suggesting that resource depletion has a more profound impact on HNA than LNA gross production. In addition, the average consumption of HNA biomass by protozoa decreased to 3.28 μg L^{-1} d^{-1}, while carbon flow resulting from LNA ingestion rose from 10% to 24% of the total protozoan metabolic consumption, signifying an increased reliance on LNA taxa during P2 compared with P1. The energy transfer ratio due to protozoan grazing (4.31 μg L^{-1} d^{-1}) and environmental resource recycling (2.55 μg L^{-1} d^{-1}) reached 1.69 during P2, exceeding that during P1 (1.43).

4. Discussion

4.1 Distinct adaptive responses of the HNA and LNA subgroups

Without an external resource supply, the bioavailable resources in the macrocosm ecosystem became increasingly scarce as the incubation progressed and they were continuously used by microbes. During P1 (days 0–16), the decline in HNA and LNA abundance suggests that both groups were constrained by the depletion of resources. The notable difference in the magnitude of decline between HNA and LNA prokaryotes indicates their distinct responses to changes in environmental conditions. It is plausible that the more significant decline in HNA populations results from their higher nutrient demands and metabolic rates, rendering them more susceptible to changes in resource availability (Mojica et al., 2020). Throughout P2 (days 16–73), both the HNA and LNA subgroups continued to decrease in abundance, albeit at a lower rate. This observation aligns with the expectation that limited resource availability will constrain prokaryotic growth. Interestingly, the LNA% and PGG-L/PGG-H continued to increase during P2, suggesting that the LNA subgroup was better adapted to cope with resource scarcity. These findings align with previous studies that demonstrated that open ocean oligotrophic communities, in contrast to coastal or shelf communities, possess a higher proportion of heterotrophic activity attributed to the LNA subgroup (Servais et al., 2003; Longnecker et al., 2005, 2006).

The distinct adaptive strategies exhibited by the HNA and LNA subgroups in response to resource availability highlight their distinct niches within aquatic ecosystems and varying contributions to ecosystem functioning under different resource conditions. The HNA subgroup, which has higher metabolic activity when resources are abundant, may be responsible for rapid resource turnover and efficient energy transfer in the food web. This tendency can be attributed to

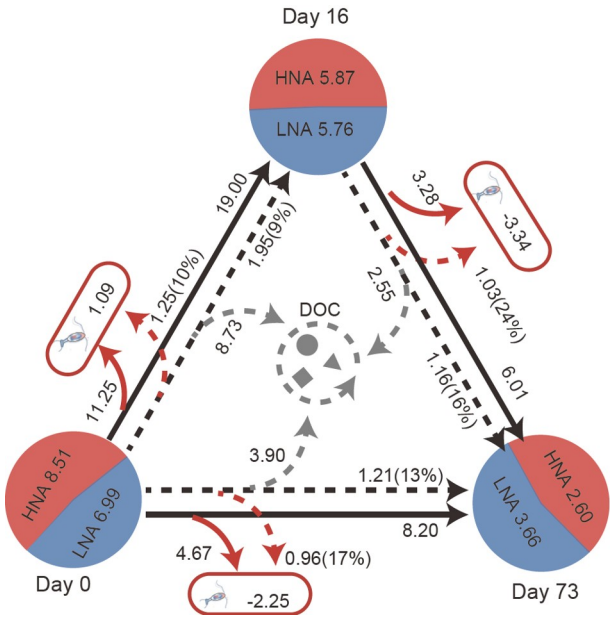

Figure 6 Carbon flow dynamics within the microbial loop. Data analysis across P1 (days 0–16) and P2 (days 16–73) highlights the shift in carbon flow. The three circles represent the prokaryotic biomass at different time (Day 0, Day 16, and Day 73), where HNA and LNA are represented in red and blue, respectively, and the numbers represent biomass (μg L^{-1}). Solid black arrows extending from each circle represent the daily average PBP-H (μg L^{-1} d^{-1}), and dashed black arrows represent PBP-L. Red arrows extending from each black arrow represent the daily average PMC (μg L^{-1} d^{-1}), where solid lines represent PMC-H and dashed lines represent PMC-L. The three red rounded rectangles represent changes in HNF biomass at different stages; for example, 1.09 in the left rectangle indicates that the HNF biomass increased by 1.09 μg L^{-1} from Day 0 to Day 16. The gray dashed arrows represent alterations in carbon flow due to other pathways, calculated as the difference between total PBP, total PMC, and the change in prokaryotic and HNF biomass. The percentages in parentheses represent the ratio of PBP and PMC of LNA to total PBP and PMC.

the higher genome complexity of HNA cells compared with LNA cells, which enables the HNA subgroup to have a higher capacity for exploiting pulses of nutrients (Azam, 1998) as well as the ability to occupy a greater variety of ecological niches (Philippot et al., 2010; Schattenhofer et al., 2011). In contrast, the LNA subgroup, being more resilient to resource scarcity, might play a crucial role in maintaining basic ecosystem functions during periods of low resource availability (Mojica et al., 2020). The compact genomes and diminished metabolic burden of replication allow LNA cells to survive under nutrient-limited conditions, ensuring the continuity of essential ecosystem processes even when resources are scarce.

4.2 Protozoan grazing preference shifts from the HNA to LNA subgroup under resource scarcity

During P1, the protozoan grazing pressure on HNA was greater than that on LNA cells, which was attributed to selective grazing by protozoa. Namely, protozoa preferentially graze HNA cells that belong to the actively growing portion of the prokaryotic assemblage (del Giorgio et al., 1996; Baltar et al., 2016), whereas the less active prokaryote subgroup, LNA cells, are less heavily grazed because of their intrinsically low metabolic rates and small size (Segovia et al., 2018). The contribution of LNA abundance to total prokaryotic abundance (LNA%) is affected by the different degrees of grazing pressure present in the environment (Tadonléké et al., 2005). The increase in LNA% during P1 might be attributed to the grazing selectivity of protozoans (primarily HNF), which favor grazing on the HNA subgroup over the LNA subgroup (Gonzalez et al., 1990; del Giorgio et al., 1996; Sintes and del Giorgio, 2014; Hu et al., 2020).

The observed changes in protozoan grazing preferences during P1 and P2 highlight the intricate relationship between microbial populations and their environment. As resources become scarce, protozoa may adapt their grazing preferences to optimally utilize available resources. The negative correlations between PMM-L/PMM-H and prokaryotic abundance and PGG-H during P2, differing from the positive correlations during P1, might indicate reduced selective grazing pressure and increased non-selective grazing pressure by protozoa (Figure 3). The RDA analysis results also support the notion that the importance of grazing selectivity decreases with resource deficiency. The shift in grazing selectivity coincides with the decreased protozoan grazing pressure on the HNA subgroup, implying that grazing selectivity diminishes under resource-limited conditions. This shift in grazing preference might be explained by the reduced food quality or availability under lower resource conditions, which are known to influence protozoan grazing rates (Monger and Landry, 1991; Christaki et al., 1998; Monger et al., 1999). Reduced food quality or availability can force grazers to adapt to alternative prey to meet their energy demands. From P1 to P2, the percentage of PBP-L allocated to protozoa increased from 69% to over 100%, revealing a marked increase in the dependency of protozoa on LNA as the resources in the incubation system became scarcer. By adjusting their grazing preferences, protozoa help maintain a balance between the HNA and LNA subgroups, ensuring the continuous operation of the microbial loop. This aligns with traditional ecological theories emphasizing the vital role of grazing in sustaining diversity (Paine, 1966).

It is noteworthy that during the transition from P1 to P2, the abundances of both HNA and LNA increased, although the former experienced more substantial growth (as evidenced by the marked decrease in LNA%). We attribute this to the significant decrease in HNF abundance, which decreased by approximately 30% and was accompanied by a nearly 50% decrease in HNF grazing pressure on the HNA subgroup (indicated by PMM-H) and little change in grazing pressure on the LNA subgroup. The persistent decline in HNF grazing pressure and abundance facilitated resource cycling (probably via cell lysis) to support the metabolic

capacity and abundance of the prokaryotic community at a lower value during the early stage of P2 (days 20–40). However, this cycling could not be sustained in the later stages of P2, resulting in a continued decline in both HNA and LNA abundances. The altered grazing preferences of protozoan grazers under resource scarcity highlight the importance of understanding the complex interactions between grazers and their prey to predict ecosystem responses to environmental changes. Such an understanding is essential for the accurate modeling of energy flow and nutrient cycling within aquatic ecosystems as well as the assessment of ecosystem stability and functioning in response to changing environmental conditions.

4.3 Implications for aquatic ecosystem functioning

The macrocosm experiment results elucidate the intricate interplay between the HNA and LNA prokaryotic subgroups and selective grazing by protozoans under declining resource availability. The projected ocean warming under global climate change is anticipated to enhance stratification and thus intensify oligotrophication in the upper ocean, leading to a deceleration of carbon cycling within the microbial loop. Although this may undermine the efficacy of the biological carbon pump and reduce energy and carbon fluxes toward the upper trophic levels, it can also promote the accumulation of refractory dissolved organic carbon, enhancing carbon sequestration in the ocean, according to the theory of the microbial carbon pump (Jiao et al., 2010, 2014, 2018). Such process may induce negative feedback on global warming associated with the accelerated release of anthropogenic CO_2.

In light of these implications, it is essential to further investigate the mechanisms driving the interactions between the HNA and LNA subgroups and protozoan grazing, as well as the responses of these subgroups to varying resource availability. Future research should also consider the potential consequences of these interactions for biogeochemical cycles and energy transfer in aquatic ecosystems, particularly under the influence of climate change and anthropogenic disturbances. A deeper understanding of these complex interactions and feedback can help researchers to better predict and manage the impacts of environmental stressors on aquatic ecosystem functioning.

5. Conclusion

In conclusion, a long-term macrocosm incubation experiment demonstrated the intricate interactions between resource availability and selective grazing by protozoans that govern prokaryotic abundance, activity, and carbon flow within the microbial loop. Our results reveal the resilience of LNA prokaryotic cells in resource-deficient conditions and their increasing contribution to carbon flow under these conditions, highlighting their importance for the stability and functioning of microbial ecosystems. Our findings also illuminate the importance of protozoa's adaptive grazing behavior in maintaining a balance between the HNA and LNA subgroups and ensuring the continuous functioning of the microbial loop. Further research is warranted to explore the underlying mechanisms of these adaptive grazing behaviors and the dynamic interplay between the HNA and LNA subgroups, as well as their implications for ecosystem processes and the global carbon cycle.

Acknowledgements *The authors wish to thank Doug Wallace, Paul Hill, Jianning Wang, Magda Waclawik, Liz Kerrigan, and Jiezhen Xie for their assistance in the experiment. This work was supported by the National Natural Science Foundation of China (Grant Nos. 42188102, 41861144018), the Natural Science Foundation of Fujian Province of China (Grant No. 2023J05017), and the Marine Economic Development Special Fund Project of Fujian Province of China (Grant No. FJHJF-L-2022-11). Chen Hu was supported by the China Postdoctoral Science Foundation (Grant No. 2021M691863). Rui Zhang was supported by the Innovation Team Project of Universities in Guangdong Province (Grant No. 2023KCXTD028). Xiaowei Chen was supported by the Ph.D. Fellowship of the State Key Laboratory of Marine Environmental Science at Xiamen University.*

Conflict of interest The authors declare that there are no conflicts of interest.

References

Azam F. 1998. Microbial control of oceanic carbon flux: The plot thickens. Science, 280: 694–696

Azam F, Fenchel T, Field J G, Gray J S, Meyer-Reil L A, Thingstad F. 1983. The ecological role of water-column microbes in the sea. Mar Ecol Prog Ser, 10: 257–263

Baltar F, Palovaara J, Unrein F, Catala P, Horňák K, Šimek K, Vaqué D, Massana R, Gasol J M, Pinhassi J. 2016. Marine bacterial community structure resilience to changes in protist predation under phytoplankton bloom conditions. ISME J, 10: 568–581

Biggs T E G, Huisman J, Brussaard C P D. 2021. Viral lysis modifies seasonal phytoplankton dynamics and carbon flow in the Southern Ocean. ISME J, 15: 3615–3622

Bouvier T, del Giorgio P A. 2007. Key role of selective viral-induced mortality in determining marine bacterial community composition. Environ Microbiol, 9: 287–297

Christaki U, Dolan J R, Pelegri S, Rassoulzadegan F. 1998. Consumption

of picoplankton-size particles by marine ciliates: Effects of physiological state of the ciliate and particle quality. Limnol Oceanogr, 43: 458–464
Edwards M, Richardson A J. 2004. Impact of climate change on marine pelagic phenology and trophic mismatch. Nature, 430: 881–884
Fukuda R, Ogawa H, Nagata T, Koike I. 1998. Direct determination of carbon and nitrogen contents of natural bacterial assemblages in marine environments. Appl Environ Microbiol, 64: 3352–3358
Gasol J M, Morán X. 1999. Effects of filtration on bacterial activity and picoplankton community structure as assessed by flow cytometry. Aquat Microb Ecol, 16: 251–264
Gasol J M, Zweifel U L, Peters F, Fuhrman J A, Hagstrom . 1999. Significance of size and nucleic acid content heterogeneity as measured by flow cytometry in natural planktonic bacteria. Appl Environ Microbiol, 65: 4475–4483
del Giorgio P A, Gasol J M, Vaqué D, Mura P, Agustí S, Duarte C M. 1996. Bacterioplankton community structure: Protists control net production and the proportion of active bacteria in a coastal marine community. Limnol Oceanogr, 41: 1169–1179
Gonzalez J M, Sherr E B, Sherr B F. 1990. Size-selective grazing on bacteria by natural assemblages of estuarine flagellates and ciliates. Appl Environ Microbiol, 56: 583–589
Hu C, Chen X, Yu L, Xu D, Jiao N. 2020. Elevated contribution of low nucleic acid prokaryotes and viral lysis to the prokaryotic community along the nutrient gradient from an estuary to open ocean transect. Front Microbiol, 11: 612053
Jiao N, Cai R, Zheng Q, Tang K, Liu J, Jiao F, Wallace D, Chen F, Li C, Amann R, Benner R, Azam F. 2018. Unveiling the enigma of refractory carbon in the ocean. Natl Sci Rev, 5: 459–463
Jiao N, Herndl G J, Hansell D A, Benner R, Kattner G, Wilhelm S W, Kirchman D L, Weinbauer M G, Luo T, Chen F, Azam F. 2010. Microbial production of recalcitrant dissolved organic matter: Long-term carbon storage in the global ocean. Nat Rev Microbiol, 8: 593–599
Jiao N, Robinson C, Azam F, Thomas H, Baltar F, Dang H, Hardman-Mountford N J, Johnson M, Kirchman D L, Koch B P, Legendre L, Li C, Liu J, Luo T, Luo Y W, Mitra A, Romanou A, Tang K, Wang X, Zhang C, Zhang R. 2014. Mechanisms of microbial carbon sequestration in the ocean—Future research directions. Biogeosciences, 11: 5285–5306
Jochem F J, Lavrentyev P J, First M R. 2004. Growth and grazing rates of bacteria groups with different apparent DNA content in the Gulf of Mexico. Mar Biol, 145: 1213–1225
Kemp P F, Cole J, Sherr B F, Sherr E B. 1993. Handbook of Methods in Aquatic Microbial Ecology. CRC Press. 213–227
Kirchman D L. 2008. Microbial Ecology of the Oceans. 2nd ed. John Wiley & Sons, Inc. 335–382
Landry M R, Hassett R P. 1982. Estimating the grazing impact of marine micro-zooplankton. Mar Biol, 67: 283–288
Landry M R, Kirshtein J, Constantinou J. 1995. A refined dilution technique for measuring the community grazing impact of microzooplankton, with experimental tests in the central equatorial Pacific. Mar Ecol Prog Ser, 120: 53–63
Li W. 1995. Composition of ultraphytoplankton in the central North Atlantic. Mar Ecol Prog Ser, 122: 1–8
Longnecker K, Sherr B F, Sherr E B. 2005. Activity and phylogenetic diversity of bacterial cells with high and low nucleic acid content and electron transport system activity in an upwelling ecosystem. Appl Environ Microbiol, 71: 7737–7749
Longnecker K, Sherr B F, Sherr E B. 2006. Variation in cell-specific rates of leucine and thymidine incorporation by marine bacteria with high and with low nucleic acid content off the Oregon coast. Aquat Microb Ecol, 43: 113–125
Marie D, Brussaard C P D, Thyrhaug R, Bratbak G, Vaulot D. 1999. Enumeration of marine viruses in culture and natural samples by flow cytometry. Appl Environ Microbiol, 65: 45–52
Menden-Deuer S, Lessard E J. 2000. Carbon to volume relationships for dinoflagellates, diatoms, and other protist plankton. Limnol Oceanogr, 45: 569–579
Mojica K D A, Carlson C A, Behrenfeld M J. 2020. Regulation of low and high nucleic acid fluorescent heterotrophic prokaryote subpopulations and links to viral-induced mortality within natural prokaryote-virus communities. Microb Ecol, 79: 213–230
Monger B C, Landry M R. 1991. Prey-size dependency of grazing by free-living marine flagellates. Mar Ecol Prog Ser, 74: 239–248
Monger B C, Landry M R, Brown S L. 1999. Feeding selection of heterotrophic marine nanoflagellates based on the surface hydrophobicity of their picoplankton prey. Limnol Oceanogr, 44: 1917–1927
Morán X A G, Lopez-Urrutia Á, Calvo-Díaz A, Li W K W. 2010. Increasing importance of small phytoplankton in a warmer ocean. Glob Change Biol, 16: 1137–1144
Painchaud J, Lefaivre D, Therriault J, Legendre L. 1996. Bacterial dynamics in the upper St. Lawrence estuary. Limnol Oceanogr, 41: 1610–1618
Paine R T. 1966. Food web complexity and species diversity. AmNaturalist, 100: 65–75
Pasulka A L, Samo T J, Landry M R. 2015. Grazer and viral impacts on microbial growth and mortality in the southern California Current Ecosystem. J Plankton Res, 37: 320–336
Pearce I, Davidson A T, Thomson P G, Wright S, van den Enden R. 2010. Marine microbial ecology off East Antarctica (30–80°E): Rates of bacterial and phytoplankton growth and grazing by heterotrophic protists. Deep Sea Res Part II-Topic Stud Oceanogr, 57: 849–862
Pernthaler J. 2005. Predation on prokaryotes in the water column and its ecological implications. Nat Rev Microbiol, 3: 537–546
Philippot L, Andersson S G E, Battin T J, Prosser J I, Schimel J P, Whitman W B, Hallin S. 2010. The ecological coherence of high bacterial taxonomic ranks. Nat Rev Microbiol, 8: 523–529
Sanders R W, Caron D A, Berninger U G. 1992. Relationships between bacteria and heterotrophic nanoplankton in marine and fresh waters: An inter-ecosystem comparison. Mar Ecol Prog Ser, 86: 1–14
Schattenhofer M, Wulf J, Kostadinov I, Glöckner F O, Zubkov M V, Fuchs B M. 2011. Phylogenetic characterisation of picoplanktonic populations with high and low nucleic acid content in the North Atlantic Ocean. Systat Appl Microbiol, 34: 470–475
Sebastián M, Auguet J, Restrepo-Ortiz C X, Sala M M, Marrasé C, Gasol J M. 2018. Deep ocean prokaryotic communities are remarkably malleable when facing long-term starvation. Environ Microbiol, 20: 713–723
Segovia B T, Meira B R, Lansac-Toha F M, Amadeo F E, Unrein F, Velho L F M, Sarmento H. 2018. Growth and cytometric diversity of bacterial assemblages under different top-down control regimes by using a size-fractionation approach. J Plankton Res, 40: 129–141
Servais P, Casamayor E O, Courties C, Catala P, Parthuisot N, Lebaron P. 2003. Activity and diversity of bacterial cells with high and low nucleic acid content. Aquat Microb Ecol, 33: 41–51
Shi Q, Wallace D. 2018. A 3-year time series of volatile organic iodocarbons in Bedford Basin, Nova Scotia: A northwestern Atlantic fjord. Ocean Sci, 14: 1385–1403
Sieburth J M N, Smetacek V, Lenz J. 1978. Pelagic ecosystem structure: Heterotrophic compartments of the plankton and their relationship to plankton size fractions 1. Limnol Oceanogr, 23: 1256–1263
Sintes E, del Giorgio P A. 2014. Feedbacks between protistan single-cell activity and bacterial physiological structure reinforce the predator/prey link in microbial foodwebs. Front Microbiol, 5: 453
Suttle C A. 2007. Marine viruses—Major players in the global ecosystem. Nat Rev Microbiol, 5: 801–812
Tadonléké R D, Planas D, Lucotte M. 2005. Microbial food webs in boreal humic lakes and reservoirs: Ciliates as a major factor related to the dynamics of the most active bacteria. Microb Ecol, 49: 325–341

Thingstad T F, Lignell R. 1997. Theoretical models for the control of bacterial growth rate, abundance, diversity and carbon demand. Aquat Microb Ecol, 13: 19–27

Unrein F, Massana R, Alonso-Sáez L, Gasol J M. 2007. Significant year-round effect of small mixotrophic flagellates on bacterioplankton in an oligotrophic coastal system. Limnol Oceanogr, 52: 456–469

Worden A Z, Follows M J, Giovannoni S J, Wilken S, Zimmerman A E, Keeling P J. 2015. Rethinking the marine carbon cycle: Factoring in the multifarious lifestyles of microbes. Science, 347: 1257594

Xiao X, Powers L C, Liu J, Gonsior M, Zhang R, Zhang L, MacIntyre H L, Chen X, Hu C, Batt J, Shi Q, Xu D, Zhang Y, Jiao N. 2022. Biodegradation of terrigenous organic matter in a stratified large-volume water column: Implications of the removal of terrigenous organic matter in the coastal ocean. Environ Sci Technol, 56: 5234–5246

Yang J, Huang S, Fan W, Warren A, Jiao N, Xu D. 2020. Spatial distribution patterns of planktonic ciliate communities in the East China Sea: Potential indicators of water masses. Mar Pollution Bull, 156: 111253

Zhang L, Chen M, Chen X, Wang J, Zhang Y, Xiao X, Hu C, Liu J, Zhang R, Xu D, Jiao N, Zhang Y. 2021. Nitrifiers drive successions of particulate organic matter and microbial community composition in a starved macrocosm. Environ Int, 157: 106776

(Editorial handling: Jianfang HU)